Ultrafast Infrared Spectroscopy of Vibrational States Prepared by Photoinduced Electron Transfer in $(CN)_5FeCNRu(NH_3)_5^-$

Chengfei Wang, Brian K. Mohney, Boris B. Akhremitchev, and Gilbert C. Walker*

Department of Chemistry, University of Pittsburgh, Pittsburgh, Pennsylvania 15260

Received: November 5, 1999

The picosecond time-resolved infrared spectra of $(CN)_5FeCNRu(NH_3)_5^-$ were collected following optical excitation and reverse electron transfer. The measured reverse electron transfer rates are greater than 3×10^{12} s^{-1}. In both formamide and deuterated water solutions, vibrational excitation in CN stretch modes is found after reverse electron transfer. The transient spectra at both earlier (1−35 ps) and later (10 ns) times give evidence of environment−solute coupling that can be accounted for by solvent heating and ion pair dynamics. A simulation of the spectral dynamics in formamide solution is presented using a kinetic model for vibrational excitation and relaxation. The simulation includes minor excitation in vibrational modes consistent with resonance Raman derived Franck−Condon factors, but it is also found that a nontotally symmetric mode is equally important as an acceptor.

Introduction

In recent years, numerous experimental and theoretical studies have addressed electron transfer (ET) reaction kinetics in solution.[1−32] Much research has focused on the role of vibration and solvent dynamics, which can control the kinetics of ET.[1] Early studies showed that the rates of ET are limited by solvation rates for certain barrierless electron transfer.[29−33] However, more recent studies showed that electron transfer rates can also far exceed the rates of diffusional solvation, which indicates critical roles for intramolecular (high frequency) vibrational modes couplings and inertial solvation.[16,28,34−36]

Mixed-valence transition-metal dimers have illustrated the interplay among inter- and intramolecular modes in ultrafast electron transfer.[7,10,20,37−39,44−45] Theoretical formulations of the thermodynamics and couplings of the thermally and optically induced electron transfer reactions of these systems were introduced by Marcus[40−42] and Hush,[38] and more recently examined by Newton and co-workers.[26] The nuclear mode couplings have been sought using resonance Raman spectroscopy, where researchers[12,15−16] have related the radiationless electron transfer rates with the resonance Raman intensities and/or absorption band shapes. Barbara and co-workers investigated the subpicosecond ET dynamics of several mixed-valence compounds in several polar solvents using femtosecond optical pump/optical probe spectroscopy.[16,36] Sumi−Marcus[6a] and Jortner−Bixon[9a,b] models were employed to predict the ET rate. Other researchers have directly studied the coupled vibrational dynamics. Woodruff and co-workers[44] utilized picosecond infrared spectroscopy to study electron transfer and vibrational excitation and relaxation both in the ruthenium ($[(CN)_5Ru^{II}CNR_UIII(NH_3)_5]^-$) and osmium ($[(CN)_5Os^{II}CNOs^{III}(NH_3)_5]^-$) dimers following optical excitation. These researchers concluded that highly excited vibrational levels of a "terminal" CN stretching mode were prepared following reverse ET, but did not distinguish the roles of different CN vibrational modes. Spears and co-workers[45] have explicitly examined vibrational mode coupling to ET in a bimolecular metal system and found that electron transfer rates were vibrational state dependent.

We report the vibrational excitations after reverse ET in a CN-bridged mixed valence complex, $[(CN)_5Fe^{II}CNRu^{III}(NH_3)_5]^-$. For simplicity, we denote this compound as FeRu. The metal−metal charge transfer (MMCT) can be represented as

$$[(CN)_5Fe^{II}CNRu^{III}(NH_3)_5]^- \underset{\text{reverse ET}}{\overset{h\nu}{\rightleftharpoons}} [(CN)_5Fe^{III}CNRu^{II}(NH_3)_5]^-$$

Optical excitation of the MMCT band corresponds to direct ET between the metal centers and is followed by reverse, thermal electron transfer from the electronically excited state(s) to the ground state. Specifically, we utilize pulsed optical (800 nm) excitation to initiate the direct ET ($Fe^{II}Ru^{III} \rightarrow Fe^{III}Ru^{II}$) and pulsed infrared (1900−2200 cm^{-1}) probe to study the consequences of the reverse ET ($Fe^{II}Ru^{III} \leftarrow Fe^{III}Ru^{II}$) reaction in deuterated water (D_2O) and formamide (FA) solvents. We have previously shown that this complex exhibits strong solvent coupling to solute vibrations upon optical charge transfer excitation.[50] Others have already reported[16,46] that the reverse thermal electron transfer in this complex occurs in ∼100 fs; in our transient infrared studies we expect to observe vibrational absorbances primarily after S_0 has been recovered.

We consider a simplified $[(CN)_5FeCNRu(NH_3)_5]^-$ geometry: $(CN)_5FeXY$ with C_{4v} symmetry, to deduce the IR and Raman active modes. We combine static spectroscopy and polarized light pump−probe data to assign the observed transient spectral features. Finally, we discuss the relationship between the observed spectral dynamics and the reverse electron transfer process.

Experimental Section

The optical pump/ infrared probe spectrometer has been introduced elsewhere.[47] The 120 fs pump pulses electronically excite the chromophore and 200 fs infrared pulses probe the vibrational states. Time-resolved IR spectra are obtained by

* To whom correspondence should be addressed.

10.1021/jp993927y CCC: $19.00
Published on Web 12/28/1999

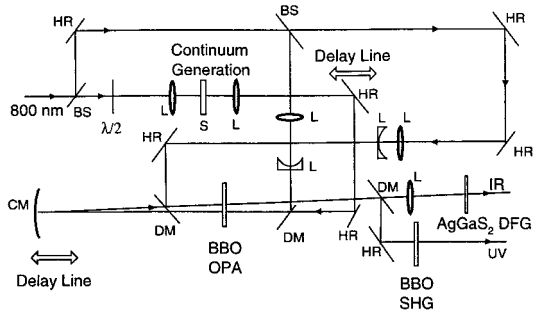

Figure 1. Schematic of mid-IR and ultraviolet light generation: HR, high reflector; BS, beam splitter; DM, dichroic mirror; L, lens; S, sapphire plate; $\lambda/2$, half-wave plate; CM, curved mirror; BBO, β-barium borate; OPA, optical parametric amplifier; SHG, second harmonic generation; DFG, difference frequency generation.

varying the relative arrival times of the pump and probe pulses at the sample. The transmitted probe pulses are detected using a monochromator and a 10-element HgCdTe array detector; the infrared spectral resolution is 7 cm^{-1}. The probe pulse repetition rate is 1.3 kHz; the pump pulse repetition rate is 0.65 kHz. The ΔOD signal {−log(IR transmission with pump) minus −log(IR transmission without pump)} is collected at 0.65 kHz.

We briefly mention our method of infrared light generation, which we have not previously reported. Infrared light is generated using an optical parametric amplifier (OPA) and difference frequency generation (DFG) (see Figure 1). The OPA is operated in a double-pass configuration. Its nonlinear optical element is a β-barium borate (BBO) crystal with a 3 mm path length and cut at 27° for type II phase-matching. The 600 μJ, 800 nm, 120 fs input pulse is split into three pulses. One pulse, a several microjoules component, is used to generate white light continuum in a 4 mm thick sapphire plate. The second pulse, comprising ca. 60 μJ, is combined with the continuum in the first pass of the OPA. Near-IR pulses are generated: a signal pulse (e.g. at 1.41 μm) and an idler pulse (e.g. at 1.85 μm). The idler pulse is reflected back into the BBO crystal for a second amplification stage, which is pumped with the remaining ~540 μJ of 800 nm light. A variable optical delay line in one arm of the second pass compensates for the optical path length mismatch between the near-IR and second 800 nm pulses. After this second pass through the BBO crystal, the amplified idler and corresponding signal pulse are focused into a $AgGaS_2$ crystal for difference frequency generation. The Ag Ga S_2 crystal (Eksma, Inc) has a 1 mm path length and is cut at 39° for type II phase-matching. By adjusting the angles of the BBO and $AgGaS_2$ crystals relative to the laser fields, we generate tunable, intense IR with central wavelengths from 4 to 8 μm and pulse durations of ca. 200 fs (fwhm).

Formamide was purchased from Aldrich and used without further purification. Deuterated water was obtained from Cambridge Isotopes. For transient absorbance measurements, the sample solution was placed in a spinning cell with thin CaF_2 windows, which provided a fresh sample volume for every laser excitation pulse. The solutions made from the sodium salt of $[(CN)_5FeCNRu(NH_3)_5]^-$ in different solvents were 0.025 M in D_2O and 0.008 M in formamide (FA). The optical path lengths of the sample cell were 0.2 mm for D_2O, and 0.75 mm for FA. The pump and probe beams were focused to 0.2 and 0.15 mm, respectively. The pump energy was 3 μJ/pulse. A half-wave plate was placed in the pump beam for polarization dependent measurements.

For static IR absorption measurements the FeRu solutions were 0.001 M in all three different solvents, D_2O, formamide (FA), and *N*-methylformamide (NMF). The optical path length was 0.1 mm.

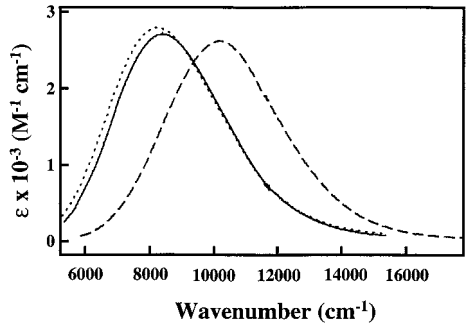

Figure 2. Charge transfer absorption spectra of FeRu in D_2O (dashed line), formamide (solid line) and *N*-methylformamide (dotted line) solvents. All three absorption bands are strongly solvent broadened.

TABLE 1: Properties of Intervalence Charge Transfer Aborption Band of FeRu in Solution

solvent	ν_{max} (cm^{-1})	$\Delta\nu_{fwhm}$ (cm^{-1})	ϵ_{max} (M^{-1} cm^{-1})	H_{ab} (cm^{-1})
D_2O	10150	4230	2640	1327
FA	8431	4008	2720	1195
NMF	8275	4057	2810	1211

Results

Figure 2 shows the metal to metal charge transfer band (MMCT) of FeRu

$$\{[(CN)_5Fe^{II}CNRu^{III}(NH_3)_5]^- \xrightarrow{h\nu} [(CN)_5Fe^{III}CNRu^{II}(NH_3)_5]^-\}$$

in three solvents. The MMCT absorption band of FeRu is centered at 10,150 cm^{-1} in D_2O, 8431 cm^{-1} in FA and 8275 cm^{-1} in NMF. It is well-known that solvent coupling can strongly influence the frequencies of the band centers and the widths of the charge transfer absorption bands.[1] The asymmetry parameter ρ defined by a log-normal fit to the optical absorption spectra is 1.316 in FA and 1.334 in NMF solution, but 1.199 in D_2O.[48]

We have estimated the electronic coupling, H_{ab}, between $Fe^{II}Ru^{III}$ and $Fe^{III}Ru^{II}$ states using the Hush−Mulliken analysis,[38,49] where

$$H_{ab} = ((4.2 \times 10^{-4})\epsilon_{max}\Delta\nu_{fwhm}\nu_{max}/d^2)^{1/2} \qquad (1)$$

Here ϵ_{max} is the maximum of extinction coefficient, $\Delta\nu_{fwhm}$ is the band full width at half-maximum, and ν_{max} is the band center frequency. The distance between the metal centers (d) is taken to be 5.2 Å. The properties of MMCT band are summarized in Table 1. We conclude that MMCT band's peak frequency and width are strongly solvent coupled, and H_{ab} is not strongly solvent dependent.

Figure 3 shows the CN vibrational stretch region of the static infrared absorption spectra of FeRu in all three solvents. The characteristics of the infrared absorption bands are summarized in Table 2. The lowest frequency infrared band in the CN stretch region is strongly influenced by the solvent.

We have previously reported the resonance Raman spectra in these solutions,[50] and the data are summarized in Table 3. The Raman intensity and frequency of the band at ca. 2000 cm^{-1} is strongly solvent dependent. A Raman excitation intensity profile across the CT band collected for FeRu in D_2O

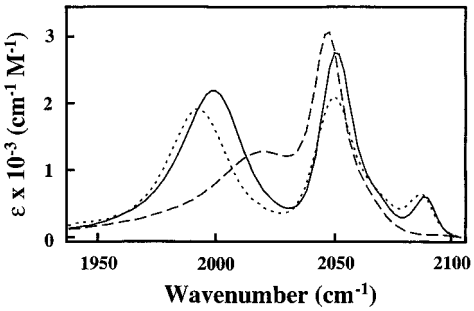

Figure 3. Static infrared absorption spectra (in CN stretch region) of FeRu in D_2O (dashed line), formamide (solid line) and *N*-methylformamide (dotted line) solvents.

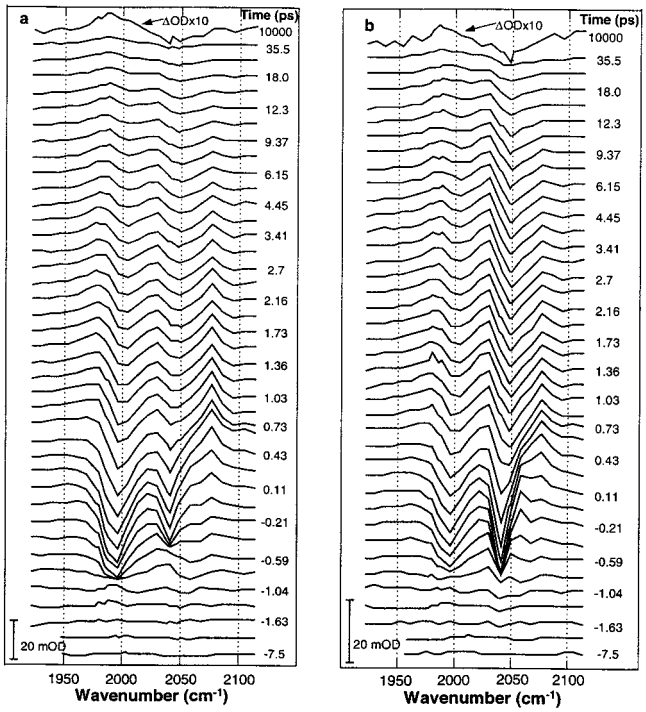

Figure 4. Time-resolved infrared difference spectra of FeRu (in CN stretch region) in formamide solvent: (a) the relative polarizations of pump (800 nm) and probe (mid-IR) pulses are parallel; (b) the relative polarizations of pump (800 nm) and probe (mid-IR) pulses are perpendicular.

TABLE 2: Properties of CN Stretch Infrared Absorption Bands of FeRu in Solution

solvent	mode	ν_{max} (cm^{-1})	$\Delta\nu_{fwhm}$ (cm^{-1})	ϵ_{max} (M^{-1} cm^{-1})
D_2O	bridge-CN	2096	7	50
D_2O	*cis*-CN	2048	14	2700
D_2O	*trans*-CN	2018	55	1404
FA	bridge-CN	2089	11	627
FA	*cis*-CN	2051	15	2771
FA	*trans*-CN	1998	32	2426
NMF	bridge-CN	2088	12	624
NMF	*cis*-CN	2050	18	2100
NMF	*trans*-CN	1993	30	2058

follows the absorption profile, indicating that a single (or degenerate) electronic transition is probed.[50]

Figure 4 shows the transient infrared difference spectra of FeRu/FA in the CN stretch regions. Negative ΔOD features correspond to loss of ground state vibrational population or cross section caused by optical excitation, and positive ΔOD features correspond to increase of vibrational population or cross section. At positive times, there are bleaches of ground state absorbances at ca. 2050 and 2000 cm^{-1}. New absorption features are seen at ca. 2085 cm^{-1}, and between 1960 and 2035 cm^{-1}.

Anisotropy measurements can provide very useful information on the relative orientations of the electronic and vibrational transition moments, and aid in determining the vibrational mode assignments. The anisotropy is calculated from the formula

$$r(t) = \frac{(I_{||} - I_{\perp})}{(I_{||} + 2I_{\perp})} \tag{2}$$

where $I_{||}$ and $I_{\perp}$ are the change in absorption intensity for the probe pulse polarized parallel and perpendicular to the optical excitation pulse, respectively.

The angle between the electronic transition moment and the vibrational transition moment can be calculated as

$$\langle \cos^2(\theta(t)) \rangle = {}^1/_3(1 + 5r(t)) \tag{3}$$

The relative polarizations of the pump and probe beams were controlled by rotating a zero-order $\lambda/2$ plate placed in the pump beam. The anisotropies at 1998 and 2051 cm^{-1} were 0.35 ± 0.03 and -0.2 ± 0.03, respectively, at 0 ps. These values of anisotropy indicate that the resonance at 1998 cm^{-1} corresponds to a mode that is approximately parallel with the charge transfer transition moment between the two metal centers. The band at 2051 cm^{-1} corresponds to a mode that is approximately perpendicular with the charge transfer transition moment. The anisotropy data are listed in Table 4.

Combining the static spectra, the time-resolved data, the anisotropy, and group theory, we can assign the absorption bands to vibrational modes. For simplicity we only consider the local C_{4v} symmetry of the $(CN)_5FeXY$ part of the binuclear complex, where XY represents the bridging CN group. Under C_{4v} symmetry the CN-based normal modes include three A_1, one B_1, and two E modes. The A_1 and E modes are IR active. The A_1, B_1, and E modes are Raman active. These modes are depicted in Figure 5.

The CN stretch mode with the highest frequency in binuclear complexes is expected to be the bridging CN mode because electron withdrawal from the lowest filled antibonding orbital of the bridging CN increases the CN bond order and hence its vibrational frequency.[51] On this basis and the observation that the 2089 cm^{-1} mode is parallel to the electronic transition, we assign the 2089 cm^{-1} mode as the bridge CN ($A_1^{(1)}$) mode. Considering that we find the transition at 2000 cm^{-1} to be parallel to the electronic transition moment, we identify this band with the $A_1^{(2)}$ (trans CN) mode. Because the 2050 cm^{-1} transition is found to be perpendicular to electronic transition moment and it is IR active, we conclude it cannot be B_1. It is either $A_1^{(3)}$ or E. The $A_1^{(3)}$ mode is the totally symmetric stretching of cis CN group modes, and the E mode should have greater IR intensity. Therefore, we assign 2050 cm^{-1} band to the E mode that is composed of cis CN stretches.

All three modes, hereafter more simply referred to only as bridge, cis, and trans, are also present in the static and transient infrared spectra of FeRu in deuterated water. Figure 6a,b shows the dynamics of FeRu in D_2O.

Discussion

We will address the following points in the remainder of this paper. First, we will discuss the evidence for the observation of the photoprepared Fe(III)Ru(II) species. Second, we will discuss the evidence for vibrational excitation in the cis and trans CN modes, and we will discuss how the excitation was achieved. Third, we will discuss the evidence that the process of photoexcitation and reverse electron transfer perturbs the

TABLE 3: Solvent Dependence of Resonance Raman Bands of $(CN)_5FeCNRu(NH_3)_5^-$

solvent[a]	mode	ν_{max} (cm^{-1})	$\Delta\nu_{fwhm}$ (cm^{-1})	band area (rel)	λ_{vib} (cm^{-1})	$\lvert\Delta a\rvert$ (Å)
D_2O	bridge-CN	2098 (1)	11 (1)	1.0	622 (20)	0.038 (0.001)
D_2O	*trans*-CN	2014 (1)	38 (2)	0.25	162 (10)	0.020 (0.001)
D_2O	Fe−C bridge	598 (1)	31 (3)	0.41	902 (30)	0.131 (0.001)
FA	bridge-CN	2089 (1)	13 (1)	0.68	453 (20)	0.033 (0.001)
FA	*trans*-CN	1996 (1)	29 (1)	0.61	428 (20)	0.034 (0.001)
FA	Fe−C bridge	592 (2)	31 (3)	0.17	408 (20)	0.089 (0.001)
NMF	bridge-CN	2089 (1)	13 (1)	0.72	505 (20)	0.035 (0.001)
NMF	*trans*-CN	1993 (1)	29 (1)	0.75	550 (20)	0.038 (0.001)
NMF	Fe−C bridge	592 (2)	33 (3)	0.28	697 (25)	0.116 (0.001)

[a] The classical reorganization energies (for modes with frequencies $<kT$) were 4550, 3560, and 3300 cm^{-1} in D_2O, formamide, and *N*-methylformamide, respectively. The driving forces were −4600, −4100, and −4000 cm^{-1} in D_2O, formamide, and *N*-methylformamide, respectively.

TABLE 4: Anisotropy Values of CN Modes of FeRu in FA

freq (cm^{-1})	anisotropy	mode assignment
2000	0.35 ± 0.03 (at 0 ps delay)	*trans*-CN
2050	−0.2 ± 0.03 (at 0 ps and positive time delay)	*cis*-CN
2085	0.34 ± 0.04 (at positive time delay)	bridge CN
2030	−0.2 ± 0.03 (at positive time delay)	$\upsilon = 1 \rightarrow \upsilon = 2$ *cis*-CN

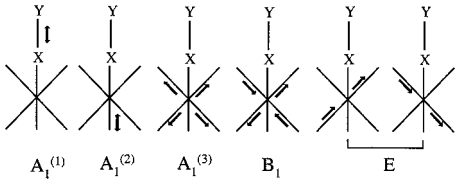

Figure 5. Vibrational modes for CN stretch region of FeRu generated using reduced symmetry, C_{4v}.

solvent environment, causing local heating and counterion dynamics. Finally, we will present a simulation of the observed spectral dynamics.

We do not directly observe the photoprepared Fe(III)Ru(II) species, which has been previously been measured to have a lifetime of <125 fs.[16,46] Fe(III)Ru(II) exhibits CN resonances that are ca. 70−100 cm^{-1} to higher frequency than the ground state Fe(II)Ru(III). The brief lifetime of $FE^{III}Ru^{II}$ causes its vibrational bands to be broad, >70 cm^{-1}. At our sensitivity these features would be hard to distinguish from transient coherence effects.[52] If the Fe(III)Ru(II) state lived even 3 times longer, we would see a distinct feature around 2130 cm^{-1}, and we do not. Thus, our transient IR data are consistent with the previously measured lifetimes of the photoinduced Fe(III)Ru(II) state. The majority of data that are seen in Figures 5 and 6 therefore reflect ground electronic state dynamics of vibrations following reverse electron transfer.

We now discuss the vibrational dynamics in more detail. In FA solutions, the anisotropy measured at 2030 cm^{-1} was −0.2 ± 0.03 at positive delay times. This value indicates that the absorption band at 2030 cm^{-1} corresponds to a mode whose transition moment is approximately perpendicular with the charge transfer transition moment, and is therefore parallel to the IR active cis (E) mode. The anharmonicity of CN modes is ca. 20 cm^{-1}.[53] Therefore, we assign the absorption at 2030 cm^{-1} to the $\upsilon = 1 \rightarrow \upsilon = 2$ vibrational transition of the cis CN mode. Figure 7 shows the absorption kinetics measured at this frequency, and an exponential fit to the data; the fit reveals that the band grows in with a 1.3 ± 0.7 ps time constant and decays with a 13 ± 3 ps time constant. The transient spectral bands in deuterated water solutions of FeRu also indicate vibrational excitation of the cis mode (see Figure 6). Similarly, the differential absorption peak at 1980 cm^{-1} for FeRu in FA reflects the excited vibrational state absorption of the trans CN mode in S_0 state. In this case, a fit to the induced absorbance at 1980 cm^{-1} decays with a 5 ± 2 ps time constant.

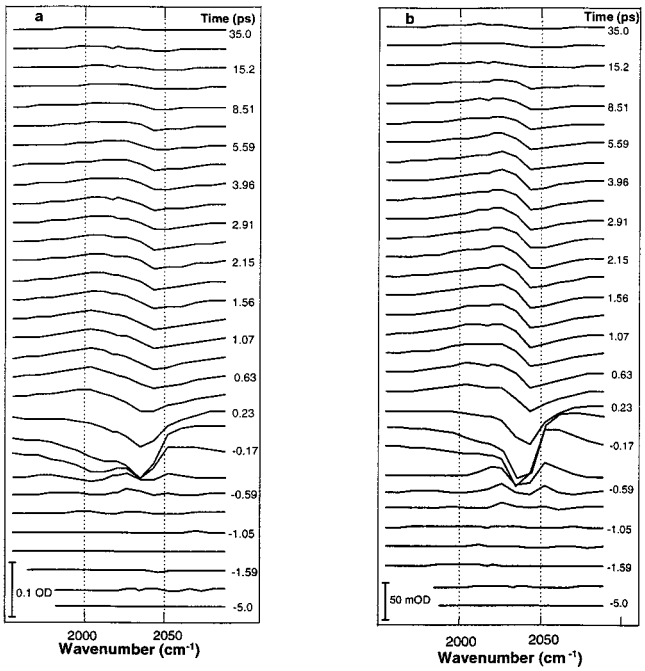

Figure 6. Time-resolved infrared difference spectra of FeRu (in CN stretch region) in D_2O solvent: (a) the relative polarizations of pump (800 nm) and probe (mid-IR) pulses are parallel; (b) the relative polarizations of pump (800 nm) and probe (mid-IR) pulses are perpendicular.

We note that we observe vibrational excitation in the cis mode, while that mode is not present in the resonance Raman data in Table 3. We now conjecture the relevance of another mechanism leading to vibrational excitation of the cis mode that includes a role for spin−orbit splitting of the $Fe^{II}Ru^{III}$ and $Fe^{III}Ru^{II}$ states. The optical transition is from d^6−Fe(II) to d^5−Ru(III); the π orbitals involved in the intervalence transition (three possible orbitals of Fe(II) and one of Ru(III)) are not the same as the π-orbitals that participate in the radiationless decay (three possible π-orbitals of Ru(II) and one π-orbital of Fe(II)); see Figure 7. Ru(III) and Fe(III) exhibit 1300 and 300 cm^{-1} spin−orbit coupling for their t_{2g} orbitals.[43b,46] We conjecture that electronic relaxation within the p manifold of Fe^{III} may be responsible for the different sets of Franck−Condon factors for the optical excitation and the radiationless, electronic ground state recovery.

We now consider whether this *cis*-CN vibrational excitation

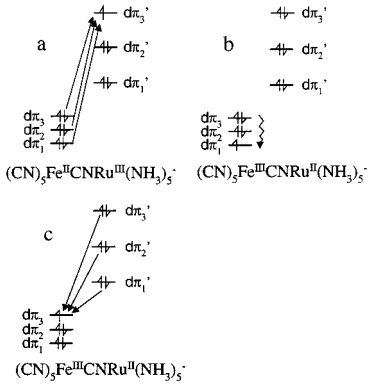

Figure 7. Spin−orbit states of FeRu and their participation in forward (optival) and reverse (radiationless) electron transfer. Relaxation within the Fe d^5 spin−orbit manifold before the reverse electron transfer causes the radiationless decay to follow a path that is different from the forward, optical process, and may account for the difference in vibronic coupling observed in the resonance Raman spectra and the vibrational state distribution observed after radiationless, reverse ET.

(2030 cm^{-1}) might be caused by vibrational energy redistribution within one electronic state. The 20 cm^{-1} vibrational line widths that set a conservative bound on the first excited vibrational state lifetime of ∼500 fs, and vibrational energy redistribution between first excited vibrational states within the ground electronic state (Fe(II)Ru(III)), would be too slow to account for the ca. 100−200 fs appearance of energy in ***cis***-CN. It is possible that IVR in $Fe^{II}Ru^{III}$ is adequately faster higher up in the vibrational potential, though we see little evidence of significant vibrational excitation. The short excited state (Fe(III)Ru(II)) lifetime causes the CN resonances to be broad (50−100 cm^{-1}) and overlapping, and thus provides little information on *cis*- to *trans*-CN vibrational energy exchange in that excited state. However, we note that the vibrational resonances of the electrochemically prepared species Fe(III)-$(CN)_5L^{2-}$ are less than 20 cm^{-1} wide.[51] The resonance Raman factors indicate modest vibrational excitation (typically no more than 1 quantum) and thus significant anharmonic couplings between vibrational modes induced by accessing highly excited vibrations in S_1 are not expected, nor is sub-100 fs vibrational energy redistribution in S_1.

In a related system, it has been suggested that Duschinsky effects are relevant or that excited and ground state normal modes may not be parallel.[42,45] We did not observe combination bands in the Raman spectra that would force us to consider Duschinsky effects for FeRu, although such effects must always be present to some degree. Other researchers[15,54] have pointed out that anharmonicities in the vibrational potential energy surfaces are pronounced in the regions where the S_0 and S_1 electronic surfaces are closest in energy, and that vibrational modes also show significant anharmonic coupling at large excitation energies. At this point, we cannot rigorously exclude either Duschinsky effects or IVR in S_0, although we sought and could not find evidence for either mechanism.

We now discuss the kinetics of the 2085, 2050, and 1998 cm^{-1} bands in FA solutions and 2085, 2050, and 2018 cm^{-1} bands in D_2O solutions. The band at 2085 cm^{-1} exhibits an anisotropy of 0.34 ± 0.04 in the transient spectra and has been assigned to the bridging CN. Again, we note that there can be no significant contribution to this feature from residual absorbance of the trans CN in Fe(III)Ru(II) because no corresponding band is seen for the cis CN at 2135 cm^{-1}. There is considerable local heating as a consequence of energy release of the radiationless decay process (ca. 12 000 cm^{-1}), and other research

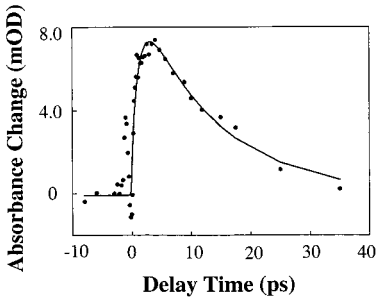

Figure 8. Transient absorption kinetics of FeRu in FA at a frequency of 2030 cm^{-1}. This absorption was assigned to the $v = 1 \rightarrow v = 2$ vibrational excited-state absorption of cis CN. Fitting an exponential model for the decay of the data yields a characteristic time of 13 ps.

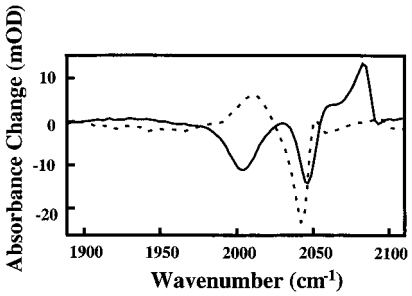

Figure 9. Temperature-dependent static infrared difference spectra of FeRu in D_2O (dotted line) and formamide (solid line) solvents, respectively. The spectra were obtained by subtracting the cold spectra (23 °C) from the hot spectra (56 °C).

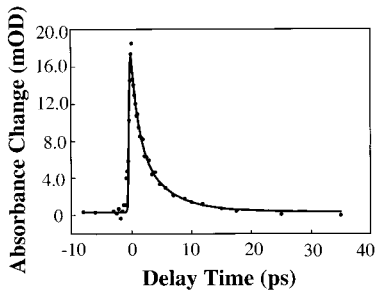

Figure 10. Transient absorption spectrum of FeRu in formamide at a frequency of 2085 cm^{-1}. The absorption band is assigned to bridging CN absorption. The decay in the band intensity is caused by local solvent/solution cooling. Fitting the feature to a decaying exponential yields a 1.3 ps time constant.

groups[1c] have shown that the local temperature decays on a ca. 1−10 ps time scale, depending on the solvent and solute. Figure 9 gives the temperature-dependent static infrared difference spectra of $[(CN)_5Fe^{II}CNRu^{III}(NH_3)_5]^-$ in FA and D_2O. We assign the picosecond time-dependent intensity of the band at 2085 cm^{-1} to local solvent heating. The decay kinetics of this band in FA are well fit with a 1.3 ± 0.7 ps time constant (see Figure 10). The exponential fit to the bleach recovery of the 1998 cm^{-1} band in FA also shows a dominant 1.9 ± 0.7 ps component, which we assign to local cooling. Apparently, the intermolecular forces that control the local temperature sensed by the trans CN mode are also sensed by the bridging mode. This is reasonable; when the dimer is made, the static spectra show an upshift of the bridge CN mode that is accompanied by a downshift of the trans CN frequency, and the trans CN is most basic.[43a] The bleach recovery of the 2050 cm^{-1} band is found to be slower, 19 ± 4 ps, which suggests a weaker solute−solvent interaction. In summary, the observed bands exhibit the consequences of solution environment changes caused by the

electron transfer processes, as well as vibrational relaxation dynamics.

The IR difference spectra at very long times (>35 ps) show a persistent bleach at 2050 cm^{-1} and induced absorbances at 2010 and 1970 cm^{-1} in D_2O and FA, respectively; see Figures 4 and 6. These features disappear with a time constant of ~10 ns. Long-lived perturbations in the solution environment can contribute to these signals. It is unlikely that the features are caused by solvent structural changes alone because the differential features seen in Figures 4, 6, and 9 do not have matching signs; FA shows a bleach at 2000 cm^{-1} in Figure 9 and an absorbance at that frequency in Figure 4. Static spectra taken with added salt (500 mM $NaClO_4$) do not exhibit significant changes in the CN vibrational resonances, though the electronic spectra shift in frequency. This suggests that, at our concentrations of FeRu, in both FA and D_2O, the mixed valence complex is ion paired with sodium. It may be that the optically induced electron transfer which moves charge away from the iron also causes the sodium counterion to move far enough away from the complex to allow a solvent molecule to occasionally slip into the void. The characteristic time for solvent-separated ion pair to reconvert to an ion pair is expected to be nanoseconds or longer.[55,56]

Simulation of the Observed Dynamics. We now present a simulation of the observed spectral dynamics. In this simulation we assume that the vibrational state distribution we observe is generated in the radiationless decay process. We note that this implies that vibrational modes that are not active in the resonance Raman spectrum are active in the reverse electron transfer. As discussed above, we speculate this occurs because the spin−orbit states that are involved in the optical absorption are not the same as the spin−orbit states involved in the reverse electron transfer, and the same Franck Condon factors should not be expected a priori to apply to the two processes. The simulation considers the cross section and population dynamics of the cis, trans, and bridging modes after electron transfer. The equations used to calculate the vibrational populations are as follows:

$$dF_{j,i}(t)/dt = k_{j,i+1}F_{j,i+1}(t) - k_{j,i}F_{j,i}(t) \quad (4)$$

$$\sum_{i=0}^{k} F_{j,i}(t) = \sum_{i=0}^{k} F_{j,i}(0) \quad (5)$$

$F_{j,i}(t)$ is the time-dependent population of vibrational state i in mode j at time t. $k_{j,i}$ is the rate constant for the population loss from state i of mode j. Invoking the harmonic oscillator approximation, we assume $k_{j,i} = ik_{j,i}$. $j = 1$ corresponds to the trans mode and $j = 2$ corresponds to the cis mode.

The transient ΔOD signal (after reverse ET) is

$$\Delta A(t,\nu) = \sum_{i=0}^{k} c_1(i+1)B_{1,i}(t,\nu)[F_{1,i}(t) - F_{1,i+1}(t)] - c_1B'_{1,0}(\nu) + \sum_{i=0}^{k} c_2(i+1)B_{2,i}(t,\nu)[F_{2,i}(t) - F_{2,i+1}(t)] - c_2B'_{2,0}(\nu) + c_3B_{3,0}(\nu)F_{3.0}(t) \quad (6)$$

Here ΔA is the induced absorbance and c_1, c_2, and c_3 are proportional to cross sections. $B_{j,i}(t,\nu)$ are Gaussian line-shape functions for one-photon absorption from state i in mode j. B' denotes the $Fe^{II}Ru^{III}$ while B denotes $Fe^{III}Ru^{II}$. The Gaussian line-shape function has the form

$$B_{j,i}(t,\nu) = (1 + f\exp(-t/\tau_1) + f_j\exp(-t/\tau_2) \times \exp(-(\nu - \nu_{j,0})^2/w_{j,0}^2) \quad (7)$$

where $\nu_{j,i}$ is band center frequency and $w_{j,i}$ is its width. f is a parameter that accounts for the temperature dependence of the cross section; it is zero for the unpumped state. τ_1 is the constant for the exponential time dependence of the cross section due to solvent cooling, while τ_2 accounts for ion pair dynamics. For these high-frequency vibration modes, the Boltzman factors place essentially all of the population in the ground vibrational state at negative times. At positive time, nonequilibrium vibrational populations are generated by optical excitation and reverse electron transfer. Within the harmonic oscillator approximation, μ_i^2 is proportional to $(i + 1)$, where μ^2 is proportional to the absorption cross section.

The anharmonicity can be calculated as[53]

$$n(n-1)h\nu_e\chi_e = nh\nu_1 - h\nu_n \quad (8)$$

$$2h\nu_e\chi_e = 2h\nu_1 - h\nu_2 = 22.6\ cm^{-1} \quad (9)$$

$$6h\nu_e\chi_e = 3h\nu_1 - h\nu_3 = 71.2\ cm^{-1} \quad (10)$$

The simulated spectra for FeRu in FA are shown in Figure 11. From the simulation, we find that, after reverse ET, the vibrational populations for *cis*-CN and *trans*-CN in S_0 are approximately 77 ± 6% in $\nu = 0$, 20 ± 5% in $\nu = 1$, 1.7 ± 0.5% in $\nu = 2$ and 1.4 ± 0.5% in $\nu = 3$ for *cis*-CN; and 75 ± 6% in $\nu = 0$, 23 ± 5% in $\nu = 1$, 2 ± 0.5% in $\nu = 2$, and ~0.0 ± 0.5% in $\nu = 3$ for *trans*-CN. A similar vibrational distribution may be used to simulate the transient difference spectra in deuterated water solution, though the solvent cooling dynamics are faster on the bridging CN and more complex on the trans CN. The vibrational excitation in the trans mode is consistent with the prediction from the resonance Raman data,[50] but the cis (nontotally symmetric mode) excitation is additional.

We find no evidence that a majority of the electronic excitation energy is deposited into a mode composed of CN stretches in the reverse electron transfer. This finding is quite different from related work on a Ru^{3+}/Ru^{2+} system.[44] Our findings differ in part because we specifically identify several distinct modes at different frequencies rather than assigning all

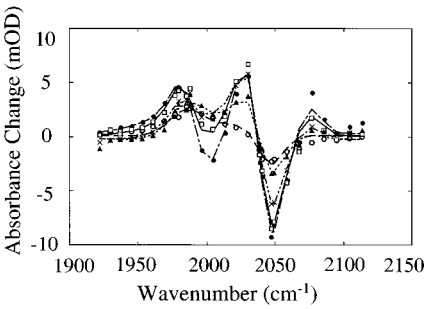

Figure 11. Actual and simulated pump−probe difference spectra of FeRu in formamide: (●) 1 ps delay data (dash−dot line is simulation); (□) 3 ps delay data (solid line is simulation); (×) 7 ps delay data (dash double dot line is simulation); (▲) 15 ps data (dotted line is simulation); (○) 35 ps delay data (dashed line is simulation). The rate constants for vibrational relaxation ($\nu = 1 \rightarrow \nu = 0$) as described in the text are 8 × 10^{-10} s^{-1} for the *cis*-CN mode, and 4 × 10^{11} s^{-1} for the *trans*-CN mode. The rate of change of the intrinsic cross section (due to solvent cooling) for the trans and bridging CN modes is 7 × 10^{-12} s^{-1}.

of the spectral dynamics to a single mode. We also identify in the spectral dynamics a role for solvent heating.

Summary

We have presented the time-resolved infrared spectra of $[(CN)_5FeCNRu(NH_3)_5]^-$ solutions following optical excitation and reverse electron transfer. The reverse electron transfer rates are faster than 3×10^{12} s^{-1}, consistent with previous observations. In both formamide and deuterated water solutions, we find excitation in a vibrational mode of the system that is nontotally symmetric in a local point group for the iron center; this mode is also not active in the ground state resonance Raman spectra. The participation of spin−orbit states that are not probed in the resonance Raman spectra is adequate to explain the observed vibrational excitation in the reverse electron transfer. The transient spectra give evidence of environment−solute coupling that can be accounted for by solvent heating and possibly ion pair dynamics. We have provided a simulation of the spectral dynamics in formamide solution, including the effects of vibrational excitation and relaxation, which accounts for the major components in the data.

Acknowledgment. We are thankful to the Hupp research group at Northwestern University for providing the FeRu sample used in these experiments. We gratefully acknowledge the Office of Naval Research (N0001-96-1-0735) and 3M Co. for financial support.

References and Notes

(1) For recent reviews in this area, see: (a) Electron Transfer From Isolated Molecules To Biomolecules, Parts 1 and 2. *Advances in Chemical Physics*; Bixon, M., Jortner, J., Eds.; Wiley: New York, 1999; Vol. 106 and 107. (b) Chen, P. Y., Meyer, T. J. *Chem. Rev.* **1998**, *98*, 1439. (c) Eisenthal, K. G. *J. Phys. Chem.* **1996**, *100*, 12997. (d) Voth, G. A.; Hochstrasser, R. M. *J. Phys. Chem.* **1996**, *100*, 13034. (e) Barbara, P. F.; Meyer, T. J.; Ratner, M. A. *J. Phys. Chem.* **1996**, *100*, 13148.

(2) Zusman, L. D. *J. Chem. Phys*. **1980**, *49*, 295.

(3) Calef, D. F.; Wolynes, P. G. *J. Phys. Chem*. **1983**, *87*, 3387.

(4) Okada, A., Chernyak, V., Mukamel, S. *J. Phys. Chem. A* **1998**, *102*, 1241 and references therein.

(5) van der Zwan, G.; Hynes, J. T. *J. Chem. Phys.* **1982**, *76*, 2993.

(6) (a) Marcus, R. A., J. Phys. Chem. B, 1998, *102*, 10071. (b) Sumi, H.; Marcus, R. A. *J. Chem. Phys.* **1986,** *84*, 4894. (c) Marcus, R. A.; Sutin, N. *Biochim. Biophys. Acta* **1985**, *811*, 265. (d) Marcus, R. A. *J. Chem. Phys*. **1956**, *24*, 966.

(7) Newton, M. D. In Electron Transfer From Isolated Molecules To Biomolecules, Part 1. *Advances in Chemical Physics*; Wiley: New York, 1999; Vol. 106, p 303. Newton, M. D.; Sutin, N. *Annu. Rev. Phys. Chem*. **1984**, *35*, 437.

(8) Hwang, J. K.; Creighton, S.; King, G.; Whitney, D.; Warshel, A. *J. Chem. Phys.* **1988**, *89*, 859.

(9) (a) Bixon, M.; Jortner, J. *Chem. Phys*. **1993**, *176*, 467. (b) Jortner J.; Bixon, M. *J. Chem. Phys*. **1988**, *88*, 167.

(10) Bader, J. S.; Kuharski, R. A.; Chandler, D. *J. Chem. Phys.* **1990**, *93*, 230.

(11) Coalson, R. D.; Evans, D. G.; Nitzan, A.*J. Chem. Phys.* **1994**, *101*, 436.

(12) (a) Myers, A. B. *Chem. Phys.* **1994**, *180*, 215. (b) Myers, A. B. *Chem. Rev.* **1996**, *96*, 911.

(13) Ladanyi, B. M., Maroncelli, M, *J. Chem. Phys*, **1998**, *109*, 3204.

(14) Nagasawa, Y.; Yartsev, A. P.; Tominaga, K.; Bisht, P. B.; Johnson, A. E.; Yoshihara, K. *J. Phys. Chem*. **1995**, *99*, 653.

(15) Wynne, K.; Galli, C.; Hochstrasser, R. M. *Adv. Chem. Phys.* **1999**, *107*, 263.

(16) Walker, G. C.; Barbara, P. F.; Doorn, S. K.; Dong, Y.; Hupp, J. T. *J. Phys. Chem*. **1991**, *95*, 5712. Reid, P. J.; Silva, C.; Barbara, P. F.; Karki, L.; Hupp, J. T. *J. Phys. Chem*. **1995**, *99*, 2609.

(17) Asahi, T.; Mataga, N. *J. Phys. Chem*. **1992**, *93*, 6575.

(18) Gould, I. R., Farid, S. *Acc. Chem. Res.* **1996**, *29*, 522.

(19) Kosower, E. M.; Huppert, D. *Annu. Rev. Phys. Chem*. **1986**, *37*, 127.

(20) Weaver, M. J.; McManis, III, G. E. *Acc. Chem. Res.* **1990**, *23*, 294.

(21) Doolen, R, Simon J. D., Baldridge K. K. *J. Phys. Chem.* **1995**, *99*, 13938.

(22) Lippert, E.; Rettig, W.; Bonacic-Koutecky, V.; Heisel, F.; Miehe, J. A. *Adv. Chem. Phys.* **1990**, *92*, 7241.

(23) Nocek, J. M.; Zhou, J. S.; DeForest, S.; Priyadarshy, S.; Beratan, D. N.; Onuchic, J. N.; Hoffman, B. M. *Chem. Rev.* **1996**, *96*, 2459.

(24) Barbara, P. F.; Jarzeba, W. *Adv. Photochem*. **1990**, *15*, 1.

(25) Maroncelli, M.; MacInnis, J.; Fleming, G. *Science* **1989**, *243*, 1674.

(26) Elliott, C. M., Derr, D. L., Matyushov, D. V., Newton, M. D. *J. Am. Chem. Soc*., **1998**, *20*, 11714. Cave, R. J., Newton, M. D. *J. Chem. Phys.* **1997,** *106*, 9213.

(27) Simon, J. D.; Su, S. G. *Chem. Phys.* **1991**, *152*, 143.

(28) Asbury, J. B.; Ellingson, R. J.; Ghosh, H. N.; Ferrere, S.; Nozik, A. J.; Lian, T *J. Phys. Chem.* B. **1999**, *103*, 3110. Ellingson, J.; Asbury, J. B.; Ferrere, S.; Ghosh, H. N.; Sprague, J. Lian, T.; Nozik, A. J. *J. Phys. Chem.* **1998**, *102*, 6455.

(29) Simon, J. D. *Acc. Chem. Res*. **1988**, *21*, 128.

(30) Bagchi, B. *Annu. Rev. Phys. Chem.* **1989**, *40*, 115.

(31) Maroncelli, M.; Fleming, G. *J. Chem. Phys.* **1988**, *89*, 5044.

(32) Gramp, G.; Harrer, W.; Hetz, G. *Ber. Bunsen-Ges. Phys. Chem.* **1990**, *94*, 1343.

(33) Fonseca, T. *Chem. Phys. Lett.* **1989**, *162*, 491.

(34) Tominaga, K.; Walker, G. C.; Jarzeba, W.; Barbara, P. F. *J. Phys. Chem*. **1991**, 95, 10475.

(35) Yoshihara, K.; Nagasawa, Y.; Yartsev, A.; Kumazaki, S.; Kandori, H.; Johnson, A. E.; Tominaga, K. *J. Photochem. Photobiol. A: Chem*. **1994**, *80*, 169.

(36) Kliner, D. A. V.; Tominaga, K.; Walker, G. C.; Barbara, P. F. *J. Am. Chem. Soc.* **1992**, *114*, 8323.

(37) Creutz, C. *Prog. Inorg. Chem*. **1983**, *30*, 1.

(38) Hush, N. S. *Prog. Inorg. Chem.* **1967**, *8*, 391.

(39) Ulstrup, J. *Charge Transfer Processes in Condensed Media*; Springer: Berlin, 1979.

(40) Marcus, R. A.; Sutin, N. *Biochim. Biophys. Acta* **1985**, *811*, 265.

(41) Britt, B. M.; Lueck, H. B.; McHale, J. L. *Chem. Phys. Lett.* **1992**, *190*, 528.

(42) Knochenmuss, R.; Muino, P. L.; Wickleder, C. *J. Phys. Chem*. **1996**, *100*, 11218.

(43) (a) Doorn, S. K,; Hupp, J. T. *J. Am. Chem. Soc.* **1989,** *111*, 1142. (b) Hupp, J. T.; Meyer, T. J. *Inorg. Chem*. **1987**, *26*, 2332.

(44) Doorn, S. K.; Dyer, R. B.; Stoutland, P. O.; Woodruff, W. H. *J. Am. Chem. Soc*. **1993**, *115*, 6398.

(45) (a) Spears, K. G.; Wen, X. Zhang, R. *J. Phys. Chem.* **1996**, *100*, 10206. (b) Spears, K. G. *J. Phys. Chem.* **1995**, *99*, 2469. (c) Wen, X.; Arrivo, S. M.; Spears, K. G. *J. Phys. Chem.* **1994**, *98*, 9693.

(46) Tominaga, K.; Kliner, D. A. V.; Johnson, A. E.; Leinger, N. E.; Barbara, P. F. *J. Chem. Phys.* **1993**, *98*, 1228.

(47) Akhremitchev, B. B.; Wang, C.; Walker, G. C. *Rev. Sci. Instrum*. **1996**, *67*, 3799.

(48) Siano, D. B.; Metzier, D. E. *J. Chem. Phys.* **1969**, 5*1*, 1856.

(49) Burewicz, A. and Haim, A. *Inorg. Chem*. **1988**, *27*, 1611.

(50) Wang, C.; Mohney, B. K.; Williams, R.; Hupp, J. T.; Walker, G. C. *J. Am. Chem. Soc*. **1998**, *120*, 5848.

(51) (a) Swanson, B. I. *Inorg. Chem.* **1976**, *15*, 253. (B) Hester R. E.; Nour, E. M. *J. Chem. Soc., Dalton Trans.* **1981**, 939.

(52) Walker, G. C.; Hochstrasser, R. M. Ultrafast Vibrational Spectroscopy: Methods, Theory,and Applications. In *Laser Techniques in Chemistry;* Wiley: New York, 1995.

(53) Durand, D.; Carmo, L. C. S.; Luty, F. *Phys. Rev. B* **1989**, *39*, 6096.

(54) Yartsev, A.; Nagasawa, Y.; Douhal, A.; Yoshihara, K., *Chem. Phys. Lett.* **1993**, *207*, 546.

(55) Das, A. K.; Tembe, B. L. *J. Chem. Phys.* **1998**, *108*, 2930.

(56) Hartman, R. S.; Knoitsky, W. M.; Waldeck, D. H. *J. Am. Chem. Soc*. **1993**, *115*, 9692.